THE JOURNAL OF PHYSICAL CHEMISTRY C

Article

Cite This: J. Phys. Chem. C 2017, 121, 19989-19998

pubs.acs.org/JPCC

Regiospecific Nucleation and Growth of Silane Coupling Agent Droplets onto Colloidal Particles

Marlous Kamp,*[,†,§] Giuseppe Soligno,[‡,§] Fabian Hagemans,[†,§] Bo Peng,[†] Arnout Imhof,[†] René van Roij,[‡] and Alfons van Blaaderen*[,†]

[†]Soft Condensed Matter, Debye Institute for Nanomaterials Science, Utrecht University, Princetonplein 1, 3584 CC Utrecht, The Netherlands

[‡]Institute for Theoretical Physics, Utrecht University, Princetonplein 5, 3584 CC Utrecht, The Netherlands

Supporting Information

ABSTRACT: Nucleation-and-growth processes are used extensively in the synthesis of spherical colloids, and more recently regiospecific nucleation-and-growth processes have been exploited to prepare more complex colloids such as patchy particles. We demonstrate that surface geometry alone can be made to play the dominant role in determining the final particle geometry in such syntheses, meaning that intricate chemical surface patternings are not required. We present a synthesis method for "lollipop"-shaped colloidal heterodimers (patchy particles), combining a recently published nucleation-and-growth technique with our recent findings that particle geometry influences the locus of droplet adsorption onto anisotropic template particles. Specifically, 3-methacryloxypropyl trimethoxysilane (MPTMS) is nucleated and grown onto bullet-shaped and nail-shaped colloids. The shape of the template particle can be chosen such that the MPTMS adsorbs regiospecifically onto the flat ends. In particular, we find that particles with a wider base increase the range of droplet volumes for which the minimum in the free energy of adsorption is located at the flat end of the particle compared with bullet-shaped particles of the same aspect ratio. We put forward an extensive analysis of the synthesis mechanism and experimentally determine the physical properties of the heterodimers, supported by theoretical simulations. Here we numerically optimize, for the first time, the shape of finite-sized droplets as a function of their position on the rod-like silica particle surface. We expect that our findings will give an impulse to complex particle creation by regiospecific nucleation and growth.

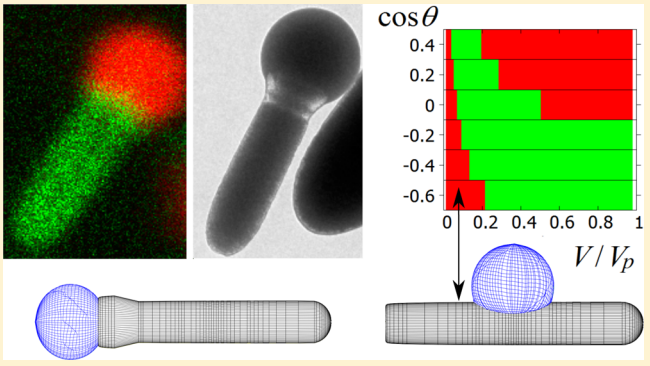

INTRODUCTION

In the past decade, complex particles have attracted a tremendous rise in interest as a result of newly invented fabrication methods to prepare such complex particles in an efficient manner, accompanied by new fundamental and industrial applications for such systems. A recent development in the creation of complex colloids is nucleation and growth onto preformed template particles, a process in which the contact angle determines the final particle shape.[1−7] In refs 3−7, the silane coupling agent 3-methacryloxypropyl-trimethoxysilane (MPTMS*) was nucleated and grown onto template particles of various shapes such as polystyrene (PS) spheres and ellipsoids; hematite cubes, disks and peanut-shaped colloids; and octadecyltrimethoxysilane (OTMS)-grafted silica spheres and clusters, in this manner yielding asymmetric PS/MPTMS*, hematite/MPTMS*, and silica/MPTMS* hybrid particles. (In this paper we indicate with an asterisk (*) behind the name of the silane coupling agent used that we are referring to the hydrolyzed and slightly condensed phase of such coupling agents. Often such hydrolyzed and slightly condensed coupling agents like MPTMS* are not soluble in pure water and separate out as liquid droplets.) In an exciting recent development,[6,7] Youssef et al. even employed a light- and pH-triggered dewetting of the MPTMS* to prepare shape-shifting colloids.

These advancements built on previous work by Sacanna, Kegel, and Philipse,[8] where it was demonstrated that magnetite particles (or silica particles[9]) and MPTMS* droplets form thermodynamically stable Pickering emulsions. The heterodimer formation in refs 3−7 takes these Pickering emulsions to the level of a single particle per emulsion droplet (or multiple droplets per particle[10−12]). Of course, complete wetting leads to a core−shell morphology and may also be desirable in certain cases.[13−15]

A next step in these nucleation-and-growth techniques is to be able to control the location of attachment of the reactant droplet onto the particle, that is, to achieve regiospecific adsorption. An obvious way to achieve this is by first creating a regiospecific surface functionalization on the template

Received: May 4, 2017
Revised: August 16, 2017
Published: August 17, 2017

DOI: 10.1021/acs.jpcc.7b04188
J. Phys. Chem. C 2017, 121, 19989−19998

particles.[16−22] For example, several researchers have exploited the fact that cetyl triammonium bromide (CTAB) binds stronger and therefore with higher density to the [100] facet (longitudinal side) of gold nanorods, allowing regiospecific functionalization of the rounded ends of the nanorods.[18−21] However, the free energy of the placement of a droplet with a certain volume at a specific location is influenced not only by any chemical surface patterning but also by the particle geometry.[22−24] Geometry can therefore also be exploited to achieve regiospecific nucleation and growth.

In previous investigations by some of us (Peng et al.[25]), methyl methacrylate was nucleated and grown regiospecifically onto the flat end of MPTMS-grafted bullet-shaped silica rods, resulting in particles sometimes referred to as having a "lollipop" shape. These experiments were combined with numerical calculations where we computed, using the Triangular Tessellation technique,[26,27] the free energy of a bullet-shaped particle adsorbed at a flat fluid−fluid interface with respect to the particle position and orientation at the interface (neglecting capillary deformation effects). This was, of course, only a first step toward correctly modeling the particle-droplet systems of the experiments because the adsorption of a colloidal particle at a finite-volume droplet rather than at a flat fluid−fluid interface can be highly affected by both the interface curvature and the capillary deformations induced by the particle on the droplet shape. Using this approximated model, we showed that, for homogeneous surface tensions of the particle with the two fluids, the free energy has a global minimum when the particle lies with its long side at the interface (edge-on adsorption configuration) and an additional local minimum when the particle has its flat end at the interface plane (end-on adsorption configuration); however, we also showed that if the surface tensions of the particle with the two fluids are opportunely tuned on the particle flat end with respect to the remaining particle surface, then the end-on configuration becomes the global minimum. Assuming that polymer nucleation is an equilibrium process, these theoretical findings suggested that the regiospecificity observed in the experiments was a combined effect of geometry and chemical heterogeneity of the particle surface. The influence of geometry was proven in a clever set of control experiments, where the droplet adsorption was observed to move from the particle flat end to the particle long side[25,28,29] after rounding off the particle edges through successive silica coatings. This same result was also confirmed by our approximated theoretical model.[25]

In this paper, we significantly improve the theoretical model in ref 25 by using a recently introduced numerical method[30] to compute the free energy of a particle adsorbed at a finite-volume droplet, including also capillary deformation effects (which, in general, can be quite important[31]). As a new result, we show that the attachment of the droplet at the particle flat end, rather than at the particle long side, can be the equilibrium configuration even if the particle has homogeneous chemical surface properties. In addition, by comparing theoretical predictions and experiments, we propose and discuss mechanisms by which the nucleation-and-growth occurs, and we investigate how small differences in the template particle's geometry affect the droplet's attachment site, proving that geometry alone can be exploited to direct the nucleation-and-growth.

Experimentally, we prepare heterodimer particles by hydrolysis and condensation of MPTMS onto OTMS-grafted rod-like silica particles. The MPTMS becomes insoluble in water and the droplets nucleate and/or attach themselves (following Wang et al.[5]) to the template particles forming "lollipop"-shaped particles. Various authors have recently described methods to control and to modify the shape of the bullet-shaped silica particles used by Peng et al.[25] and that were developed in our group,[28] for example, by regulation of the growth temperature,[32] by manipulating the reagent addition time,[33] or by exploiting a gradient in etching rate.[34,35] In particular, Datskos and Sharma[32] showed that changing the temperature of the reaction mixture during particle growth changes the growth speed and thus the particle diameter. We demonstrate that nail-shaped template particles sustain "lollipop"-shaped heterodimer formation at much larger aspect ratios than do bullet-shaped template particles. By changing the template geometry we thus reach unprecedented control over this chemical system.

EXPERIMENTAL SECTION

Chemicals. The following chemicals were used. Silane coupling agents: (3-methacryloxypropyl)trimethoxysilane (MPTMS, ≥ 98%, Sigma-Aldrich), octadecyltrimethoxysilane (OTMS, 90%, technical grade, Aldrich), and (3-aminopropyl)-triethoxysilane (APTES, ≥ 98%, Sigma-Aldrich). Surfactants: Pluronic F108 block copolymer surfactant (average mol. wt.: 14 600 g/mol, BASF), Igepal CO-520 (average mol. wt.: 441 g/mol, Aldrich), and Triton X-100 (laboratory grade, Sigma-Aldrich). Water was deionized with a Millipore Direct-Q UV3 reverse osmosis filter apparatus (Millipore Corporation) and had a resistivity of at least 18.2 MΩ cm. Ethanol (absolute) was obtained from Merck and 1-pentanol (ReagentPlus, ≥99%) from Sigma-Aldrich. The catalysts aqueous ammonia (26.6 wt %), *n*-butylamine (99.5 wt %), and sodium citrate dihydrate (p.a. ≥ 99.0%, anhydrous) were purchased from Sigma-Aldrich. 2,2′-Azobis(2-methylpropionitrile) (AIBN) initiator from Janssen Chimica was recrystallized from ethanol. RAS (rhodamine isothiocyanate-aminostyrene) dye conjugate was prepared as described in ref 36 and dissolved in acetone (99%, Merck) to a final concentration of ∼0.2 mg/mL. Fluoresceine isothiocyanate (FITC, ≥90 wt % (HPLC)) was purchased from Sigma-Aldrich, as was polyvinylpyrrolidone (PVP, K-30, 40 000 g/mol). All chemicals were used as received.

Synthesis of Asymmetric ("Lollipop") Silica/MPTMS* Heterodimers. Nail-shaped particles were prepared using regulation of the growth temperature, as recently published in ref 32, based on the original work of Kuijk et al.[28] Specifically, 1 g of PVP (40 000 g/mol) was dissolved in 10 mL of pentanol by sonication in a 20 mL glass vial (Wheaton). To this solution, 1 mL of ethanol, 0.28 mL of water and 67 μL of sodium citrate solution (0.18 M in water) were added. After shaking the vial by hand, 0.225 mL of ammonia was added and the vial was shaken again. Finally, 100 μL of TES was added and the vial was shaken once more. The reaction mixture was immediately placed in an oven thermostated at 50 °C. Performing the reaction at elevated temperature reduces the rod diameter, as described in ref 32. After 2 h in the oven, the bottle was placed in a fridge at 4 °C to grow the nails' wider "head". After 6−18 h, ethanol was added to quench the reaction, and the nail-shaped particles were collected by centrifugation and redispersion in ethanol. This synthesis method was also successfully repeated on a larger scale (150 mL of PVP/pentanol mixture, in a 250 mL round-bottomed flask).

The nail-shaped particles were optionally labeled with FITC dye[28,29] and then grafted with OTMS before the MPTMS*

DOI: 10.1021/acs.jpcc.7b04188
J. Phys. Chem. C 2017, 121, 19989−19998

condensation step. For dye-labeling, a mixture of 4 mg FITC, 4 μL of APTES, and 250 μL of ethanol was allowed to form APTES-dye conjugates for 2 h under stirring. To 8.5 mg of dried nail-shaped particles we added 1 mL of ethanol, 10 μL of ammonia, and 40 μL of dye solution. After 2 h, the dyed particles were centrifuged and washed two times with water. For the OTMS-grafting step, the nail-shaped particles were dried once more, and a mixture of 1 mL of toluene, 0.1 mL of butylamine, and 0.1 mL of OTMS was added. After 2 h of sonication and overnight reaction, the dye-labeled and OTMS-grafted nail-shaped particles were washed twice with ethanol.

For the MPTMS* nucleation and growth step, nail-shaped particles (~8.5 mg) were dried and redispersed in a mixture of 890 μL of water and 355 μL of F108 in water (0.35 wt %). To this dispersion, 1.25 μL of ammonia and 18 μL of MPTMS were added. The dispersion was stirred for 30 min, during which an MPTMS* protrusion nucleated and grew onto the nail-shaped particles. The final MPTMS*-heterodimer particles were collected by centrifuging twice with water and then stored in ethanol.

To fluorescently label the MPTMS* droplets, after the MPTMS* had reacted for 1 h under magnetic stirring, 20 μL of the solution of RAS in acetone was added to the reaction mixture and the mixture was stirred for an extra 10 min. The RAS in acetone is taken up by the MPTMS* droplets, making the MPTMS* droplets suitable for confocal microscopy studies.

Asymmetric heterodimer particles were also prepared from rod-like particles with a flat end (bullet-shaped particles). To this end, the exact same synthesis route as above was performed on bullet-shaped particles synthesized, as described in ref 28.

The MPTMS* droplet can also be cross-linked through its organic functional groups by a free radical polymerization reaction. Typically, 2.8 mg OTMS-grafted nail-shaped particles were dispersed in 0.88 mL of deionized water and 0.34 mL of Pluronic F108 solution (0.35 wt % in water) by sonicating for 2 h. Then, 1 μL of ammonia (26.6 wt %) and 18.75 μL of MPTMS were added. After stirring this reaction mixture for 1 h, 7 mg AIBN was added. The mixture was heated to 70 °C for 24 h and subsequently washed with absolute ethanol (100%) several times until no scattering from secondary nucleation was visible in the supernatant.

Transmission Electron Microscopy. Samples were prepared by drying a droplet of heterodimer dispersion on Formvar- and carbon-coated transmission electron microscopy (TEM) grids (copper, 200 mesh, Electron Microscopy Sciences); for preparation, see ref 37. Electron microscopy images were recorded on an FEI Tecnai T12 microscope at 120 kV acceleration voltage. HAADF-STEM imaging was performed on a Tecnai 20 FEG (FEI company) at 200 kV.

Confocal Microscopy. Confocal images were recorded on a Leica SP8 confocal microscope. The microscope was equipped with a Leica HCX Plan Apo STED Orange 100× oil immersion lens (NA = 1.4), which is a lens optimized for use in stimulated emission depletion (STED), mode although STED was not required. Excitation wavelengths of 495 and 543 nm were selected from the spectrum of a white light laser by means of an acousto-optical beam splitter (AOBS). Two detectors recorded the fluorescent signals in different wavelength ranges: a photomultiplier tube (PMT) in the range 510−540 nm for the FITC-dyed particle cores and a "HyD" detector (from Leica Microsystems) in the range 565−700 nm for the RAS-dyed MPTMS* protrusion. The latter detector is a combination of a PMT and a system similar to an avalanche photodiode, which makes the HyD a more sensitive detector with a low dark noise and a large dynamic range. The two channels were displayed in different 8-bit color look-up tables: green (FITC-labeled core) and red (RAS-dyed protrusion).

Numerical Calculations. A numerical method was used to calculate the equilibrium shape and position of droplets attached to colloidal particles. The fluid−fluid interface between the droplet and the external fluid (i.e., the fluid surrounding both particle and droplet) is treated as a 2D curved surface with no thickness and is represented by a grid of points (an illustrative sketch of the grid used is shown in Figure S1). Given as input parameters the particle shape, the droplet volume, and Young's contact angle, the position of the fluid−fluid interface grid points that minimizes the free energy of the system is the equilibrium shape of the fluid−fluid interface, that is, the solution of the Young−Laplace Equation with Young's Law as boundary condition.[30] To compute the minimum-energy position of the fluid−fluid interface grid points, we use a simulated annealing algorithm, that is, a Monte Carlo method. A detailed description of the algorithm's numerical implementation for 2D systems can be found in ref 30 and for 3D systems in ref 38. This numerical method, applied here to study droplets attached at nontrivially shaped colloidal particles, is very well suited as well to study droplets wetting heterogeneous substrates[39] and colloidal particles adsorbed at fluid−fluid interfaces.[31,40]

The droplet attachment position on the colloidal particle is chosen as an input parameter, and then the droplet equilibrium shape is computed by constraining the droplet to remain around this initial position (to impose this constraint, the vertical axis of the fluid−fluid interface grid is kept fixed in the Monte Carlo simulation; see Figure S1). For a given droplet volume, we repeat this calculation sampling different initial positions of the droplet on the particle, identifying, finally, the droplet position corresponding to the droplet equilibrium shape with minimum free energy. The free energy F of the particle-droplet-external fluid system is

$$F = \gamma S + \gamma_1 W_1 + \gamma_2 W - V\Delta P \tag{1}$$

where γ, γ_1, and γ_2 are the droplet-external fluid, particle-external fluid, and particle-droplet surface tensions, respectively; S, W_1, and W are the surface areas of, respectively, the droplet-external fluid, particle-external fluid, and particle-droplet interface; V is the droplet volume; and ΔP is the difference between the bulk pressure of the droplet and the bulk pressure of the external fluid. Note that we are neglecting gravity effects, as they are not relevant in the experimental systems of interest. Using $\Sigma \equiv W_1 + W$ to indicate the total particle surface area, we rewrite eq 1 as

$$F = \gamma(S - W\cos\theta) - V\Delta P + \Sigma\gamma_1 \tag{2}$$

where we introduced $\cos\theta = (\gamma_1 - \gamma_2)/\gamma$ using Young's Law, with θ Young's contact angle taken inside the droplet. The term $\Sigma\gamma_1$ is a constant and therefore it can be ignored. The term $V\Delta P$ is also not relevant in our analysis because we will compare the energies of droplets with the same V and ΔP, attached at different positions on the particle surface. So we write the free energy as $E \equiv F - \Sigma\gamma_1 + V\Delta P$, that, is F (eq 1) shifted by a constant, obtaining

$$E = \gamma(S - W\cos\theta) \tag{3}$$

DOI: 10.1021/acs.jpcc.7b04188
J. Phys. Chem. C 2017, 121, 19989−19998

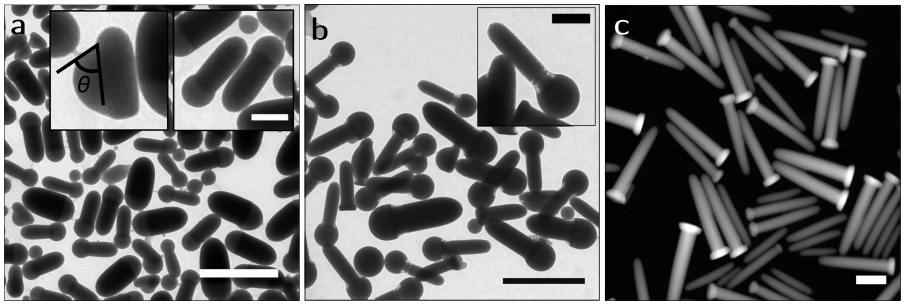

Figure 1. TEM images of heterodimer particles prepared from various silica templates. These images show heterodimers prepared by nucleation and growth of MPTMS* onto OTMS-grafted (a) short bullet-shaped particles (aspect ratio $m = 2.1 \pm 0.1$, with standard deviation $\sigma_m = 0.4$) and (b) intermediate length nail-shaped particles ($m = 3.2 \pm 0.1$, $\sigma_m = 0.5$). The insets in panels a and b are zoomed-in images of the heterodimers and of a heterodimer in which the contact angle of the MPTMS onto the template particle is indicated. The slight etching of the nail-shaped particles visible in panel b is a result of the presence of ammonia in the nucleation and growth and cross-linking reaction.[34] (c) HAADF-STEM micrograph of nail-shaped particles prepared by temperature-regulated growth. Scale bars represent: (a,b) 2 and (c) 1 μm; insets: 500 nm.

To sum up our numerical method, we compute, by minimizing E (eq 3) with Monte Carlo simulations, the equilibrium shape of a droplet attached at a colloidal particle of a certain shape, given as input parameters the droplet volume V, the droplet initial position on the particle surface, and Young's contact angle θ. During the simulation, the droplet is numerically constrained to remain around its initial position (so we find the minimum energy shape that the droplet has in the given position at the particle surface). By sampling different initial positions of the droplet on the particle surface, we find, at fixed θ and V, the position on the particle surface where the droplet equilibrium shape has minimum E, which is the equilibrium configuration of the particle-droplet system.

The shapes of the colloidal particle that we considered in our calculations are a nail of aspect ratio $m = 5.8$, a bullet of aspect ratio $m = 6.0$, and a bullet of aspect ratio $m = 2.1$ (see Figure 3). The aspect ratio m of each particle shape is defined as the ratio of the end-to-end distance in the long direction of the particle with the diameter of the particle circular section taken at the center. The exact definition of these particle shapes is reported in the Supporting Information. For numerical convenience, in our model the nail head does not contain edges as sharp as in the TEM images. This negligibly affects the results, as, we will show, it is the diameter of the circular flat base of the particle that plays a major role in the physics of the system. In our calculations, we compute the equilibrium shape of the droplet attached at the flat end and attached at the long side of these particle shapes.

RESULTS AND DISCUSSION

Particle Synthesis and Characterization. In a recent publication,[5] Wang and coworkers showed that hydrophobized (spherical) silica particles can serve as a template for the nucleation and growth of a silane coupling agent (SCA), MPTMS*. An OTMS-grafting on the silica in combination with a surfactant (Pluronic F108) is used to create a suitable contact angle, such that the MPTMS* does not fully envelope the silica colloid but instead adsorbs partially onto the template particle. In this way, a dumbbell with two lobes of different chemical compositions is formed: a heterodimer (see Figure S2). The MPTMS* lobe can be polymerized further through the methacrylate groups in a radical polymerization reaction using a suitable initiator. It is interesting to note that the connection between the silica lobe and the MPTMS* lobe is not effectuated by covalent bonds, as the OTMS layer does not provide binding sites for the MPTMS* and also acts as a steric barrier for the MPTMS* to reaching the remaining surface silanol groups. Hence, the bonding between the two lobes is expected to be mainly a geometrical envelope of the silica by the MPTMS* or possibly the result of a large enough contact area between the silica and the MPTMS* droplet for sufficient adsorption free energy.

Bullet-shaped particles were prepared according to the method of Kuijk et al.[28] MPTMS* nucleation and growth onto such bullet-shaped particles of aspect ratio $m = 2.1 \pm 0.1$ successfully yielded asymmetric dumbbells ("lollipops") (see Figure 1a), a result similar to that in the work by Peng and coworkers.[25] The contact area between particle and droplet is sufficiently large in terms of the adsorption free energy to regiospecifically direct the placement of the droplets and stabilize the particle, as will be supported by the calculations presented in the next section. Note that in some particles the locus of MPTMS* condensation is on the long side of the silica bullets; we estimate a heterodimer yield of 78 ± 2%. On closer inspection (Figure S3), side-on attachment is often caused by the lack of a flat end on smaller rods, which is due to loss of the emulsion droplet—from which the bullet grows—before all TES has reacted, which happens for some of the rods. For bullet-shaped colloids of aspect ratio $m = 6.2 \pm 0.2$ (with standard deviation $\sigma_m = 1$), a similar synthesis resulted in composite particles for which the locus of condensation was on the long side for virtually all template particles (Figure S4). That is, the locus of adsorption is not only dependent on contact angle but also on the particle aspect ratio, in line with previous observations.[41]

To investigate the influence of small changes in the template particle geometry on the heterodimer formation, we produced nail-shaped particles by the temperature-regulated growth technique of Datskos and Sharma.[32] These nail-shaped templates have a slightly broader "nail head" at the flat end. Nail-shaped templates of aspect ratio $m = 3.2$ successfully yielded asymmetric dumbbell particles upon nucleation, growth, and cross-linking of MPTMS* (Figure 1b). In fact, the synthesis mechanism was successful for nail-shaped templates of aspect ratio up to $m = 5.8$ (as in Figure 1c and Figure 2), contrary to the case of bullet-shaped templates of $m = 6.2$. Longer nail-shaped silica particles with $m = 8.6$ did fail to deliver lollipop-shaped particles (Figure S5). These results, as summarized in Table1, indicate that the presence of a "nail head" increases the range of aspect ratios for which locus of

DOI: 10.1021/acs.jpcc.7b04188
J. Phys. Chem. C 2017, 121, 19989−19998

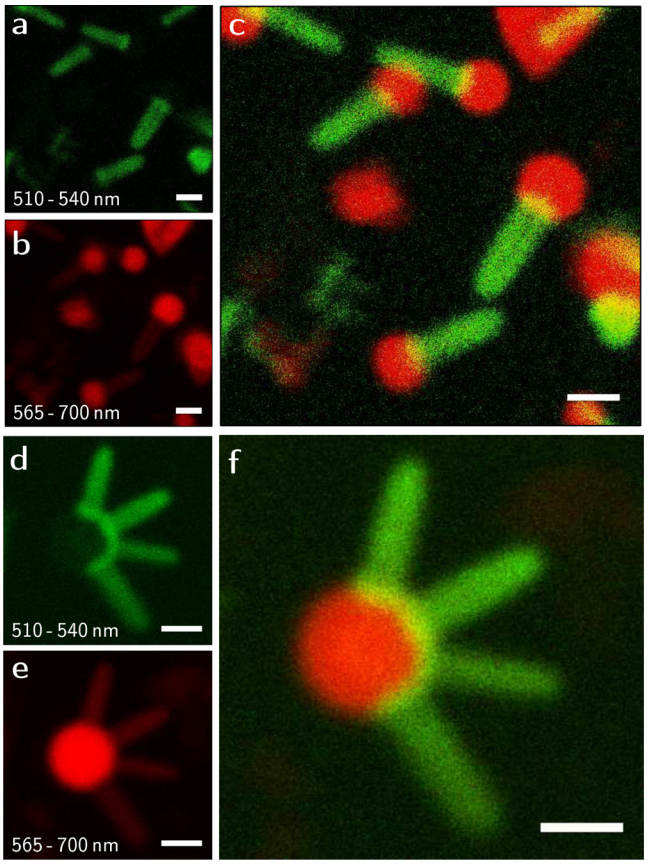

Figure 2. Confocal micrographs of asymmetric heterodimers prepared from nail-shaped silica particles. (a–c) Confocal images of loose asymmetric heterodimers templated on the silica nail-shaped particles in Figure 1c: (a) channel recording at 510–540 nm (around the emission maximum of FITC dye), (b) channel recording at 565–700 nm (around the emission maximum of RAS dye, although some bleed-through from the FITC dye can be observed), and (c) overlay of both imaging channels. The scale bars denote 1 μm. (d–f) Encountered particle assembly of multiple nail-shaped particles attached to a single MPTMS* droplet. (d) Channel recording at 510–540 nm (around the emission maximum of FITC dye), (e) channel recording at 565–700 nm (around the emission maximum of RAS dye), and (f) overlay of both imaging channels. The scale bars denote 1 μm. A HAADF-STEM image of the nail-shaped particles is in Figure 1c.

condensation is at the flat end. The nail shape acts as a stabilizer for the nucleation-and-growth process.

As a control study, we prepared template particles with a secondary rim in the middle according to ref 35. Nucleation and growth of MPTMS* onto these particles, in the same way as described above, resulted in a droplet enveloping the end of the template particle while terminating on the middle rim (Figure S6), albeit with low particle yield. The enveloping of the first cone increases the free energy of adsorption on account of the large contact area. This synthesis further demonstrates our control over the nucleation-and-growth process.

The presented asymmetric heterodimers are suitable for fluorescence microscopy. Figure 2a–c displays confocal micrographs of particles prepared by MPTMS* nucleation and growth onto dyed and OTMS-grafted nail-shaped particles. The MPTMS* lobes were fluorescently labeled by infiltration of another dye derivative. In the FITC dye channel (Figure 2a), the locations of the nail heads are visible, and comparison with the composite image (Figure 2c) reconfirms that the MPTMS* nucleated onto the nail heads. Occasionally a small extra MPTMS* droplet nucleated onto the edge of the rod (Figure S7) when the position at the flat end was already occupied by another droplet. The preferred adsorption at the flat ends is also apparent from the occasional droplets with multiple rods attached (Figure 2d–f), although it is not immediately clear whether several heterodimers have fused together by their MPTMS* droplets during nucleation and growth or whether nail-shaped particles attached to an existing heterodimer. In either case, it again appears energetically favorable for the nail-shaped particles to stay attached to the droplet end-on rather than edge-on.

Two causes for the end-on attachment of the MPTMS* onto bullet-shaped and nail-shaped particles can be conjectured: the geometry of the templates (influencing the morphology of an attached droplet) or a difference in surface tension of the material on the long side and on the flat end of the template particles. A compositional difference in surface tension cannot explain the observation that nail-shaped particles, and bullet-shaped particles of similar aspect ratio do not yield heterodimers of equal shape. Theoretical calculations (vide infra) were performed to further investigate our hypothesis that nucleation and growth at the flat end is dominated by particle geometry.

Theoretical Calculations on the Formation Mechanism. The morphologies of a particle-droplet system were predicted theoretically by calculating the minimum free energy configuration, with the numerical method described in the Numerical Calculations section. The full results for the difference in the (free) energy E (eq 3) for the droplet equilibrium shape at different positions on the colloidal particle surface, as obtained by our numerical calculations, are reported Figures S10–S12, in units of $\Sigma\gamma$ (where Σ is the colloidal particle surface area and γ is the fluid–fluid surface tension between the droplet and the external fluid). An estimate of $\Sigma\gamma$ in units of k_{BT} is provided in Table S1 for typical experimental values. These results for the (free) energy E (eq 3) of droplets attached to nail-shaped particles of aspect ratio m = 5.8 (Figure 3a) and bullet-shaped particles of aspect ratios m = 6.0 and m = 2.1 (Figure 3b,c) are summarized in Figure 3d–f in the form of phase diagrams in the Young's contact angle θ–droplet volume V plane, for $0.1V_p \leq V \leq 1.0V_p$, where V_p is the particle volume and $-0.6 \leq \cos\theta \leq 0.4$.

As a general result, the composite droplet-particle shapes show the following behavior: droplets with a volume on the order of the particle volume ($\sim 1.0V_p$) as well as droplets that are small compared with the particle volume ($\approx 0V_p - 0.2V_p$)

Table 1. Summary of the Droplet Locations on the Template Particle As Observed in Experimental Syntheses, for Template Particles of Various Aspect Ratio m and for Different Shapes of the Template Particle (Bullet Shape or Nail Shape)

droplet location	small m (bullet: 2.1, nail: 3.2)	intermediate m (bullet: 6.2, nail: 5.8)	large m (bullet: 8.6, nail: 10.2)
bullet shape	end	edge	edge
nail shape	end	end	edge

DOI: 10.1021/acs.jpcc.7b04188
J. Phys. Chem. C 2017, 121, 19989–19998

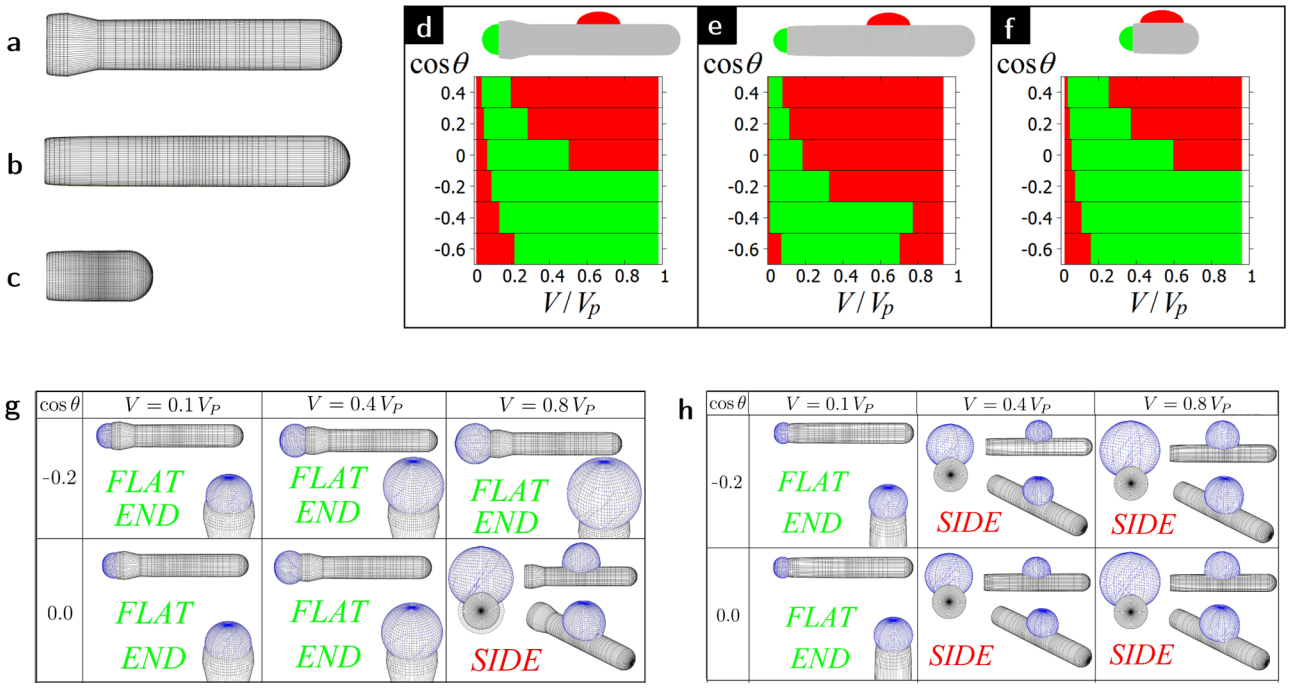

Figure 3. (a–c) Model shapes used in the simulations: (a) Nail-shaped particle with aspect ratio 5.8, (b) bullet-shaped particle with aspect ratio 6.0, (c) bullet-shaped particle with aspect ratio 2.1. (d–f) cos θ–V phase diagrams, where V is the droplet volume expressed in units of the particle volume V_p and θ is Young's contact angle (inside the droplet), based on the results in Figures S10–S12. The red areas indicate cos θ–V combinations for which the droplet prefers to attach at the long side of the particle (i.e., corresponding to $\Delta E < 0$ in Figures S10–S12). The green areas indicate cos θ–V combinations for which the droplet prefers to attach to the flat end of the particle (i.e., corresponding to $\Delta E > 0$ in Figures S10–S12). Each graph in panels d–f refers to the particle shape in panels a–c, respectively. Possible combinations for the surface tensions γ, γ_1, and γ_2 to obtain a certain cos θ are shown in Table S2. These phase diagrams prove that by solely slightly tuning the template particle geometry it is possible to direct the droplet nucleation-and-growth process. In panels g and h, we show 3D views of the droplet equilibrium shape (as obtained numerically from our method), attached at the particle in the position with minimum energy, for $V = 0.1V_p$, $0.4V_p$, $0.8V_p$ and cos $\theta = -0.2$, 0.0, for the particle shape in panels a and b, respectively. Analogous plots of the droplet equilibrium shape for a wider range of cos θ are shown for these two particle shapes in Figures S13 and S14, respectively, and for the particle shape in panel c in Figure S15.

have a high probability to adhere to the long side of the particle, while there is a middle range of droplet volumes for which the droplet's preferred location is the particle's flat end. The energy differences between the droplet configuration at the particle's flat end and at the particle's long side are on the order of 10^4 to 10^6 kT for typical experimental parameters (see Table S1), implying a strong preferential adsorption to either the flat end or the long side. Moreover, the preferred configuration of the assembly is strongly dependent on Young's contact angle. Focusing on the different template particle shapes, the bullet-shaped particle of aspect ratio 2.1 (Figure 3c) displays a broader range of cos θ–V combinations than the bullet-shaped particle of aspect ratio 6.0 (Figure 3b) for which the preferred location for the droplet is on the particle flat end, as shown in Figure 3e,f. For bullet-shaped particles of different aspect ratio but with the same surface graftings, we therefore expect the particles of larger aspect ratio to have relatively fewer droplets attached to the flat ends. This prediction is corroborated by our experimental findings where the synthesis of lollipop-shaped particles was successful using bullet-shaped particles with m = 2.1 but not using bullet-shaped particles of aspect ratio m = 6.0. Our predictions are also in agreement with the experimental results of Peng et al.,[25] who quote cos $\theta = -0.4$ and aspect ratio m = 1.9 for their template particles for which successful formation of asymmetric heterodimers was reported. Interestingly, the nail-shaped particle (Figure 3a) also has a broader range of cos θ–V combinations than the bullet-shaped particle of similar aspect ratio (Figure 3b) for which the droplet location at the flat end is energetically favored (green phase in Figure 3d–f). Thus for particles with an aspect ratio around m = 6.0, the nail shape increases, with respect to the bullet shape, the range of droplet volumes for which a "lollipop" shape forms during nucleation and growth.

We propose the following explanation for the stabilizing effect of the nail shape. A droplet attached at a flat solid surface has a spherical cap shape (Figure S16), with the contact angle imposed by Young's Law, as this is the droplet shape with minimal surface area. However, if the solid surface is curved, then the shape of the droplet attached to the solid deviates from a spherical cap because that shape cannot fulfill the boundary conditions imposed by Young's Law on the contact angle between the fluid–fluid interface and the solid surface anymore. Therefore, small droplets prefer to attach at the particle flat end, in this way keeping a spherical shape. By increasing the droplet volume, the diameter of the spherical cap exceeds the flat end's diameter at a certain droplet volume, and the droplet is forced to deviate from the spherical cap geometry. The droplet shape on the long side of the particle eventually becomes energetically favorable over the droplet shape at the flat end. The nail-shaped particles, on account of their wider base than the bullet-shaped particles, have a higher number of combinations of V and θ such that the droplet can keep a spherical cap shape and therefore such that it prefers to stay attached at the flat end. It is important to note that the droplet volumes in these calculations are expressed as a fraction of the particle volume, and hence it is not the absolute value of

DOI: 10.1021/acs.jpcc.7b04188
J. Phys. Chem. C 2017, 121, 19989–19998

the base diameter that influences the stability of the droplet but rather its value compared with the particle volume. This notion explains why the locus of droplet adsorption is consistent within each heterodimer sample even if the template particles have some polydispersity in width.

These theoretical results also provide insights into the formation mechanism of the asymmetric heterodimers. Because the theory calculates the equilibrium shape of the droplet on the particle, the droplets must have a way of sampling/exploring the differences in local surface tension. Possible ways of sampling the local surface tension are by moving over the surface of the rods until the droplet reaches a local minimum in the adsorption free energy, by Ostwald ripening, or by other droplet growth processes that involve exchange of soluble monomers through the solvent.[34] A combination of these pathways is also possible. In all of these cases, the pathways would be prevented if the droplet had already formed a branched network at the time of nucleation and was in a gel state, as proposed in ref 5. Gelation would inhibit any dissolving of the droplet or any motion over the particle surface. Hence, we conclude that the MPTMS* is primarily a liquid during the initial nucleation, possibly containing oligomers but not exhibiting extensive branching. This conclusion is also in full agreement with the recent beautiful results on "shape-shifting" colloids.[6,7]

Contact line pinning could potentially play a role in our synthesis mechanism, as it could keep a droplet stuck in a metastable configuration, without allowing it to go to the minimum energy configuration we predict. In 2016, Wang et al.[42,43] showed that contact line pinning plays an important role in particle adsorption at interfaces. Specifically, the authors mention that surface roughness for silica particles and polymer "hairs" for polymer particles can act as pinning sites. Our grafted silica template particles likely have both types of surface corrugation. The synthesis mechanism therefore falls directly into the logarithmic relaxation regime observed by the Manoharan group (unlike pinning of macroscopic droplets on macroscopic surfaces), although we consider microscopic droplets rather than adsorption at a liquid interface. Possibly, pinning is responsible for those particles in Figure 1a,b, for which droplets attached on the long side despite the template having a flat end.

Comparison between Experimental and Theoretical Results. From the occasional droplet attached to the long sides of particles shown in Figure 1a, a Young's contact angle of 63 ± 1° was inferred (with standard deviation 7°, cos θ = 0.45 ± 0.02) for MPTMS* on OTMS-grafted silica in the presence of Pluronic F108 surfactant. For this Young's contact angle, our calculations in Figure 3d–f predict that the range of droplet volumes for which adsorption at the flat end is energetically favorable is roughly twice as broad for nail-shaped particles as for bullet-shaped particles of the same aspect ratio. The extended droplet volume range exists for small droplets on the order of $0.1V_p$, explaining why droplets in the nucleation stage attach preferentially to the flat end for nail-shaped particles. It becomes apparent that the rod-like particles do accommodate droplets of larger volume than $0.1V_p$ at the flat end when examining Figures 1a,b and 2. We speculate that perhaps the dynamics of larger droplets slows down as eventually the SCA forms oligomers—a phenomenon related to pinning. The slow droplet dynamics will trap the droplet in the position at the flat end. Such a scenario also explains the droplet spillover seen on some of the particles, as seen for example in the inset of Figure 1a.

The existence of a heterogeneous contact angle, that is, a different Young's contact angle on the long side and on the flat end of the particles, cannot be excluded entirely. Droplets attached to the flat end, however, cannot provide reliable information on the Young's contact angle because these droplets can grow beyond their Young's contact angle before relocating to the long side becomes energetically favorable. For example, in Figure 1a, droplets attached to the flat ends display an average opening angle of 97 ± 2° with a standard deviation of 12% (cos θ = −0.13 ± 0.03) with the flat end. If indeed the flat ends exhibit a larger Young's contact angle, then our calculations predict an even wider range of droplet volumes that can be accommodated at the flat end for nail-shaped particles compared with bullet-shaped particles (Figure 3d–f). A homogeneous contact angle is, however, expected: The grafting with OTMS should have eliminated any differences in carbon chain density at the surface because the radius of curvature for our particles is much larger than of molecular size, as in the case of the gold nanorods mentioned in the Introduction. Our experimental and theoretical results are in perfect agreement for a homogeneous contact angle of 63 ± 7°. The results thus indicate that adsorption at the flat end is purely a geometric effect.

As a control study with the purpose of varying the surface tension of the nucleating agent, we investigated the nucleation and growth of a mixture of MPTMS* and mercaptopropyltrimethoxysilane* (mercapto-PTMS*) onto nail-shaped particles (Figure 4). For low (25%) volume fractions of mercapto-

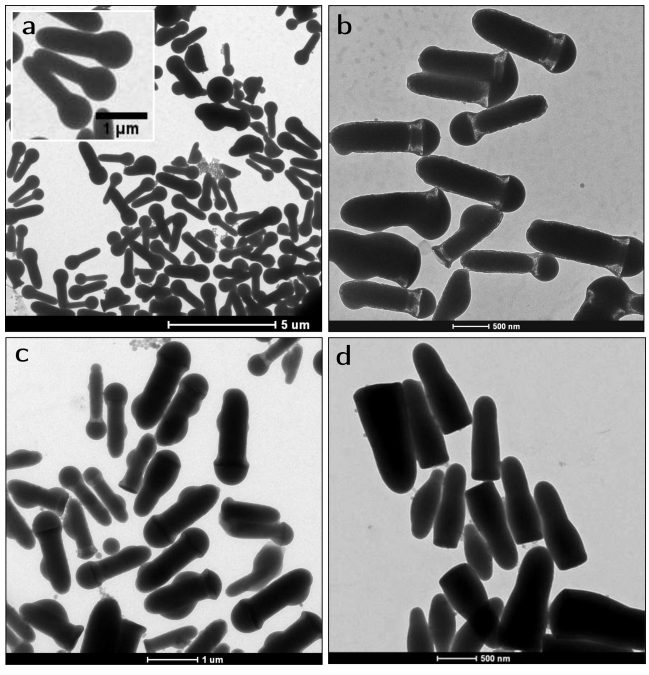

Figure 4. Nucleation and growth of mixed SCAs. TEM micrographs of lollipop-shaped heterodimers prepared from OTMS-grafted nail-shaped particles by nucleation and growth of mixtures of the silane coupling agents MPTMS* and mercapto-PTMS*. (a) 0% v/v mercapto-PTMS. (b) 25% v/v mercapto-PTMS. (c) 50% v/v mercapto-PTMS. (d) 100% v/v mercapto-PTMS. The slight etching of the template particles visible in panel b is due to the presence of ammonia in the reaction mixture during heterodimer synthesis.

DOI: 10.1021/acs.jpcc.7b04188
J. Phys. Chem. C 2017, 121, 19989−19998

PTMS, the geometry of the heterodimers remained intact. For 50% mercapto-PTMS, droplets nucleated partially onto the flat ends and partially onto the remainder of the template particles. For pure (100%) mercapto-PTMS, the droplets are located on the long sides of the template particles as a broad droplet (or possibly as an enveloping ring). In short, with increasing mercapto-PTMS* volume fraction, it becomes energetically favorable for the droplet to attach to the long side. Because the surface tensions against water are similar for these two compounds (see ref 44, although the data are for silane-modified silicas, while the surface tensions for hydrolyzed and slightly polymerized droplets may differ), the cause of the morphological change must be a gradual change in Young's contact angle. The morphologies in Figure 4b,c are not well described by our theory as we do not consider the possibility of droplet breakup into an end-on and edge-on attached mass. For the droplets on the long sides of the particles in Figure 4d we measure a Young's contact angle of 18 ± 2° ($\cos\theta = 0.95 \pm 0.01$), a value for which the side-on adsorption is indeed favored for any droplet volume according to our theoretical calculations (Figure 3d). Mercapto-PTMS is interesting for future applications on account of its thiol groups, which could bind many kinds of (catalytic) nanoparticles,[45−47] making these heterodimers suitable for purposes such as heterogeneous catalysis.

Conversely, one might ask whether surface graftings other than OTMS could be employed on the silica rods. As shown in Figure 3d−f, the largest stable droplet volume range exists for nucleating silane coupling agents that do not wet the template surface well ($\cos\theta < 0$). Therefore, a more hydrophobic grafting, for example, by using a fluorinated silane coupling agent, should accommodate larger nucleating droplet sizes. Sufficient hydrophobization was indeed important as we observed fewer droplets attached to the flat end of the bullets and nails when the OTMS-grafting was carried out for a short (0.5−2 h) reaction time. On the contrary, a more hydrophilic "grafting" such as MPTMS itself (or no grafting at all) would be an interesting way to covalently couple the nucleating silane coupling agent to the template particle. In initial experiments on spherical templates with an MPTMS grafting (and without any grafting), the present synthesis route, however, yielded silica/MPTMS* heterodimers that had only slightly eccentric geometries (Figure S8). The surfactant used in the synthesis route can also be exploited to use hydrophilic surface graftings. Already when we performed the synthesis with the surfactants Igepal CO-520 and Triton X-100 instead of Pluronic F108, the nucleation and growth step resulted in heterodimers with a more desorbed MPTMS* lobe, as seen by confocal microscopy and TEM, respectively (Figure S9). A hydrophilic grafting on the template particle in combination with a surfactant/nucleating agent with long carbon chains to provide sufficient hydrophobicity is a viable subject for future research.

SUMMARY AND CONCLUSIONS

The nucleation and growth of hydrolyzed and slightly condensed/polymerized MPTMS onto bullet-shaped and nail-shaped OTMS-grafted silica particles resulted in asymmetric ("lollipop") silica/MPTMS* heterodimer colloids, with the MPTMS* droplet attached only to the flat ends of the template particles. For an aspect ratio $m = 6$, nail-shaped particles displayed a much higher "lollipop"-shaped heterodimer yield than bullet-shaped template particles. The methacryloxy groups of the MPTMS* lobes on dumbbell-shaped and asymmetric heterodimer particles were successfully cross-linked by free radical polymerization, yielding particles resilient to drying. The MPTMS* lobes were labeled with a dye derivative different from the labeled silica rods for confocal microscopy imaging.

Our experimental results are further substantiated by theoretical calculations where we numerically minimize the free energy to predict the most favorable position of a droplet on a template particle, assuming that the regiospecific nucleation-and-growth is an equilibrium process. The theoretical results indicated that, for a given Young's contact angle, a broader range of droplet volumes can be stably adsorbed at the flat end either by decreasing the template particle's aspect ratio or by fashioning a small "nail head" onto the template particles. Also, the calculations showed that the largest volume ranges for droplet attachment at the flat end occur when the droplet Young's contact angle with the particle is >90°. By using mixtures of silane coupling agents, we indeed confirmed experimentally that low Young's contact angles do not successfully form asymmetric heterodimers. Both theory and experiments thus point at the formation mechanism being an equilibrium process, at least initially. We therefore conclude that the MPTMS* droplet is liquid-like as opposed to gel-like during nucleation; that is, it contains only small oligomers.

In conclusion, we use regiospecific nucleation and growth to design new complex colloids, exploiting the particle geometry to direct the regiospecific attachment. We show by both experiments and theory how differences in the morphology link to improvements in the particle yield, and we expect that these findings will motivate further research into complex particle creation by regiospecific nucleation and growth. Second, the theoretical calculations were performed for finite-volume droplets and including capillary deformation effects, significantly improving our theoretical model in ref 25, where particles at an always-flat fluid−fluid interface were considered. Finally, droplets from SCAs allow for many more functionalizations than purely organic droplets (such as PMMA, PS, as presented by us before[25]). The current method for inorganic/organic hybrid particles could be selectively modified or extended to other nucleating SCAs (including vinyl, phenyl, and thio-based ones).

ASSOCIATED CONTENT

Supporting Information

The Supporting Information is available free of charge on the ACS Publications website at DOI: 10.1021/acs.jpcc.7b04188.

Supplementary Figures including TEM images of heterodimers prepared with template particles with different surface graftings, of different aspect ratio, and with different surfactants. Supplementary Theoretical Results including free energies and 3D equilibrium droplet shape as a function of droplet volume for different template particles. Supplementary Methods. Supplementary References. (PDF)

AUTHOR INFORMATION

Corresponding Authors

*M.K.: E-mail: M.Kamp@uu.nl.

*A.v.B.: E-mail: A.vanBlaaderen@uu.nl.

ORCID

Marlous Kamp: 0000-0003-4915-1312

Giuseppe Soligno: 0000-0003-2360-2082

Fabian Hagemans: 0000-0002-4748-8547

DOI: 10.1021/acs.jpcc.7b04188
J. Phys. Chem. C 2017, 121, 19989−19998

Arnout Imhof: 0000-0002-7445-1360
Alfons van Blaaderen: 0000-0003-3090-2753

Author Contributions

[§]M.K., G.S., and F.H. contributed equally. A.v.B. developed the concept. M.K. performed syntheses and experiments and wrote the manuscript. F.H. completed the experimental work. G.S. performed theoretical calculations. B.P. shared essential knowledge on the synthesis and characterization of lollipop-shaped PMMA/silica heterodimers. A.v.B., A.I., and R.v.R. supervised research. All authors discussed the results and commented on the manuscript.

Notes

The authors declare no competing financial interest.

■ ACKNOWLEDGMENTS

Joost de Graaf and Marjolein Dijkstra are thanked for discussions on theoretical calculations of solid particles at liquid interfaces. Hans Meeldijk is thanked for making the HAADF-STEM pictures and Jissy Jose for preparation of the RAS dye derivative. M.K. and F.H. received financial support from the Nederlandse Organisatie voor Wetenschappelijk Onderzoek (NWO) (ECHO grants 700.58.025 (M.K.) and 712.013.005 (F.H.)). Additionally, funding was received from the European Research Council under the European Unions Seventh Framework Programme (FP/2007-2013)/ERC Grant Agreement no. 291667 "HierarSACol". G.S. and R.v.R. acknowledge financial support by the "Nederlandse Organisatie voor Wetenschappelijk Onderzoek" (NWO) Vici Grant and by the Marie Curie Initial Training Network "Soft Matter at Aqueous Interfaces" (SOMATAI). This work is part of the D-ITP consortium, a program of the NWO that is funded by the Dutch Ministry of Education, Culture and Science (OCW).

■ REFERENCES

(1) Seh, Z. W.; Liu, S.; Zhang, S.-Y.; Bharathi, M. S.; Ramanarayan, H.; Low, M.; Shah, K. W.; Zhang, Y.-W.; Han, M.-Y. Anisotropic Growth of Titania onto Various Gold Nanostructures: Synthesis, Theoretical Understanding, and Optimization for Catalysis. *Angew. Chem., Int. Ed.* **2011**, *50*, 10140−10143.
(2) Sun, Y. Interfaced Heterogeneous Nanodimers. *Nat. Sci. Rev.* **2015**, *2*, 329−348.
(3) Sacanna, S.; Rossi, L.; Pine, D. J. Magnetic Click Colloidal Assembly. *J. Am. Chem. Soc.* **2012**, *134*, 6112−6115.
(4) Sacanna, S.; Korpics, M.; Rodriguez, K.; Colón-Meléndez, L.; Kim, S.-H.; Pine, D.-J.; Yi, G. R. Shaping Colloids for Self-Assembly. *Nat. Commun.* **2013**, *4*, 1−6.
(5) Wang, Y.; Wang, Y.; Zheng, X.; Yi, G.-R.; Sacanna, S.; Pine, D. J.; Weck, M. Three-Dimensional Lock and Key Colloids. *J. Am. Chem. Soc.* **2014**, *136*, 6866−6869.
(6) Youssef, M.; Hueckel, T.; Yi, G.-R.; Sacanna, S. Shape-Shifting Colloids via Stimulated Dewetting. *Nat. Commun.* **2016**, *7*, 12216.
(7) Zheng, X.; Liu, M.; He, M.; Pine, D. J.; Weck, M. Shape-Shifting Patchy Particles. *Angew. Chem., Int. Ed.* **2017**, *56*, 5507−5511.
(8) Sacanna, S.; Kegel, W. K.; Philipse, A. P. Thermodynamically Stable Pickering Emulsions. *Phys. Rev. Lett.* **2007**, *98*, 158301.
(9) Kraft, D. J.; de Folter, J. W. J.; Luigjes, B.; Castillo, S. I. R.; Sacanna, S.; Philipse, A. P.; Kegel, W. K. Conditions for Equilibrium Solid-Stabilized Emulsions. *J. Phys. Chem. B* **2010**, *114*, 10347−10356.
(10) Datskos, P.; Cullen, D. A.; Sharma, J. Step-by-Step Growth of Complex Oxide Microstructures. *Angew. Chem., Int. Ed.* **2015**, *54*, 9011−9015.
(11) Li, D.; Zhao, B.; Long, Y.; Yang, G.; Tung, C.-H.; Song, K. Preparation and Enhanced Catalytic Activity of Amphiphilic Rambutan-Like Micro-Reactors. *RSC Adv.* **2015**, *5*, 74362−74365.
(12) Zhao, B.; Li, D.; Long, Y.; Yang, G.; Tung, C.-H.; Song, K. Modification of Colloidal Particles by Unidirectional Silica Deposition for Urchin-Like Morphologies. *RSC Adv.* **2016**, *6*, 32956−32959.
(13) Schärtl, W. Crosslinked Spherical Nanoparticles with Core-Shell Topology. *Adv. Mater.* **2000**, *12*, 1899−1908.
(14) Ghosh Chaudhuri, R.; Paria, S. Core/Shell Nanoparticles: Classes, Properties, Synthesis Mechanisms, Characterization, and Applications. *Chem. Rev.* **2012**, *112*, 2373−2433.
(15) Li, G. L.; Möhwald, H.; Shchukin, D. G. Precipitation Polymerization for Fabrication of Complex Core-Shell Hybrid Particles and Hollow Structures. *Chem. Soc. Rev.* **2013**, *42*, 3628−3646.
(16) Grzelczak, M.; Vermant, J.; Furst, E. M.; Liz-Marzán, L. M. Directed Self-Assembly of Nanoparticles. *ACS Nano* **2010**, *4*, 3591−3605.
(17) Burrows, N. D.; Vartanian, A. M.; Abadeer, N. S.; Grzincic, E. M.; Jacob, L. M.; Lin, W.; Li, J.; Dennison, J. M.; Hinman, J. G.; Murphy, C. J. Anisotropic Nanoparticles and Anisotropic Surface Chemistry. *J. Phys. Chem. Lett.* **2016**, *7*, 632−641.
(18) Shibu Joseph, S. T.; Ipe, B. I.; Pramod, P.; Thomas, K. G. Gold Nanorods to Nanochains: Mechanistic Investigations on Their Longitudinal Assembly. *J. Phys. Chem. B* **2006**, *110*, 150−157.
(19) Jones, S. T.; Taylor, R. W.; Esteban, R.; Abo-Hamed, E. K.; Bomans, P. H. H.; Sommerdijk, N. A. J. M.; Aizpurua, J.; Baumberg, J. J.; Scherman, O. A. Gold Nanorods with Sub-Nanometer Separation using Cucurbit[n]uril for SERS Applications. *Small* **2014**, *10*, 4298−4303.
(20) Nie, Z.; Fava, D.; Kumacheva, E.; Zou, S.; Walker, G. C.; Rubinstein, M. Self-Assembly of Metal-Polymer Analogues of Amphiphilic Triblock Copolymers. *Nat. Mater.* **2007**, *6*, 609−614.
(21) Wu, B.; Liu, D.; Mubeen, S.; Chuong, T. T.; Moskovits, M.; Stucky, G. D. Anisotropic Growth of TiO_2 onto Gold Nanorods for Plasmon-Enhanced Hydrogen Production from Water Reduction. *J. Am. Chem. Soc.* **2016**, *138*, 1114−1117.
(22) Zhang, Z.; Pfleiderer, P.; Schofield, A. B.; Clasen, C.; Vermant, J. Synthesis and Directed Self-Assembly of Patterned Anisometric Polymeric Particles. *J. Am. Chem. Soc.* **2011**, *133*, 392−395.
(23) Doermbach, K.; Pich, A. Facile Synthesis of Dumbbell-Shaped Multi-Compartment Nanoparticles. *Nanoscale* **2015**, *7*, 9169−9173.
(24) Sun, Y.; Chen, M.; Zhou, S.; Hu, J.; Wu, L. Controllable Synthesis and Surface Wettability of Flower-Shaped Silver Nanocube-Organosilica Hybrid Colloidal Nanoparticles. *ACS Nano* **2015**, *9*, 12513−12520.
(25) Peng, B.; Soligno, G.; Kamp, M.; de Nijs, B.; de Graaf, J.; Dijkstra, M.; van Roij, R.; van Blaaderen, A.; Imhof, A. Site-Specific Growth of Polymer on Silica Rods. *Soft Matter* **2014**, *10*, 9644−9650.
(26) de Graaf, J.; Dijkstra, M.; van Roij, R. Triangular Tessellation Scheme for the Adsorption Free Energy at the Liquid-Liquid Interface: Towards Nonconvex Patterned Colloids. *Phys. Rev. E* **2009**, *80*, 1−19.
(27) de Graaf, J.; Dijkstra, M.; van Roij, R. Adsorption Trajectories and Free-Energy Separatrices for Colloidal Particles in Contact with a Liquid-Liquid Interface. *J. Chem. Phys.* **2010**, *132*, 1−14.
(28) Kuijk, A.; van Blaaderen, A.; Imhof, A. Synthesis of Monodisperse, Rodlike Silica Colloids with Tunable Aspect Ratio. *J. Am. Chem. Soc.* **2011**, *133*, 2346−2349.
(29) Kuijk, A.; Imhof, A.; Verkuijlen, M. H. W.; Besseling, T. H.; van Eck, E. R. H.; van Blaaderen, A. Colloidal Silica Rods: Material Properties and Fluorescent Labeling. *Part. Part. Syst. Charact.* **2014**, *31*, 706−713.
(30) Soligno, G.; Dijkstra, M.; van Roij, R. The Equilibrium Shape of Fluid-Fluid Interfaces: Derivation and a New Numerical Method for Young's and Young-Laplace Equations. *J. Chem. Phys.* **2014**, *141*, 1−13.
(31) Soligno, G.; Dijkstra, M.; van Roij, R. Self-Assembly of Cubes into 2D Hexagonal and Honeycomb Lattices by Hexapolar Capillary Interactions. *Phys. Rev. Lett.* **2016**, *116*, 258001.
(32) Datskos, P.; Sharma, J. Synthesis of Segmented Silica Rods by Regulation of the Growth Temperature. *Angew. Chem., Int. Ed.* **2014**, *53*, 451−454.

DOI: 10.1021/acs.jpcc.7b04188
J. Phys. Chem. C 2017, 121, 19989−19998

(33) Datskos, P.; Chen, J.; Sharma, J. Addressable Morphology Control of Silica Structures by Manipulating the Reagent Addition Time. *RSC Adv.* **2014**, *4*, 2291−2294.
(34) Hagemans, F.; van der Wee, E. B.; van Blaaderen, A.; Imhof, A. Synthesis of Cone-Shaped Colloids from Rod-Like Silica Colloids with a Gradient in the Etching Rate. *Langmuir* **2016**, *32*, 3970−3976.
(35) Hagemans, F.; Vlug, W.; Raffaelli, C.; van Blaaderen, A.; Imhof, A. Sculpting Silica Colloids by Etching Particles with Nonuniform Compositions. *Chem. Mater.* **2017**, *29*, 3304−3313.
(36) Bosma, G.; Pathmamanoharan, C.; de Hoog, E. H. A.; Kegel, W. K.; van Blaaderen, A.; Lekkerkerker, H. N. W. Preparation of Monodisperse, Fluorescent PMMA-Latex Colloids by Dispersion Polymerization. *J. Colloid Interface Sci.* **2002**, *245*, 292−300.
(37) Bozzola, J. J.; Russell, L. D. *Electron Microscopy: Principles and Techniques for Biologists*; Jones & Bartlett Learning: Burlington, MA, 1999.
(38) Soligno, G. *Capillary Interactions and Self-Assembly from the Equilibrium Shape of Fluid-Fluid Interfaces*; Ph.D. Thesis, Utrecht University, 2017.
(39) Devic, I.; Soligno, G.; Dijkstra, M.; van Roij, R.; Zhang, X.; Lohse, D. Sessile Nanodroplets on Elliptical Patches of Enhanced Lyophilicity. *Langmuir* **2017**, *33*, 2744−2749.
(40) Vis, M.; Opdam, J.; van 't Oor, I. S. J.; Soligno, G.; van Roij, R.; Tromp, R. H.; Erné, B. H. Water-in-Water Emulsions Stabilized by Nanoplates. *ACS Macro Lett.* **2015**, *4*, 965−968.
(41) Lewandowski, E. P.; Searson, P. C.; Stebe, K. J. Orientation of a Nanocylinder at a Fluid Interface. *J. Phys. Chem. B* **2006**, *110*, 4283−4290.
(42) Wang, A.; Rogers, B.; Manoharan, V. N. Effects of Contact-Line Pinning on the Adsorption of Nonspherical Colloids at Liquid Interfaces. arXiv:1607.08167 [cond-mat.soft].
(43) Wang, A.; McGorty, R.; Kaz, D. M.; Manoharan, V. N. Contact-Line Pinning Controls How Quickly Colloidal Particles Equilibrate with Liquid Interfaces. *Soft Matter* **2016**, *12*, 8958−8967.
(44) Plueddemann, E. P. *Silane Coupling Agents*; Springer Science & Business Media, New York, 1982; p 96.
(45) Colvin, V. L.; Goldstein, A. N.; Alivisatos, A. P. Semiconductor Nanocrystals Covalently Bound to Metal Surfaces with Self-Assembled Monolayers. *J. Am. Chem. Soc.* **1992**, *114*, 5221−5230.
(46) Ben Haddada, M.; Blanchard, J.; Casale, S.; Krafft, J.-M.; Vallée, A.; Méthivier, C.; Boujday, S. Optimizing the Immobilization of Gold Nanoparticles on Functionalized Silicon Surfaces: Amine- vs Thiol-Terminated Silane. *Gold Bull.* **2013**, *46*, 335−341.
(47) Chomette, C.; Duguet, E.; Mornet, S.; Yammine, E.; Manoharan, V. N.; Schade, N. B.; Hubert, C.; Ravaine, S.; Perro, A.; Treguer-Delapierre, M. Templated Growth of Gold Satellites on Dimpled Silica Cores. *Faraday Discuss.* **2016**, *191*, 105−116.

DOI: 10.1021/acs.jpcc.7b04188
J. Phys. Chem. C 2017, 121, 19989−19998